

Please fill in the name of the event you are preparing this manuscript for.	SPE Virtual Improved Oil Recovery Conference
Please fill in your 6-digit SPE manuscript number.	SPE-209354-MS
Please fill in your manuscript title.	"Tailing" Phenomenon During Polymer Propagation At The Milne Point Polymer Flood

Please fill in your author name(s) and company affiliation.

Given Name	Middle Name	Surname	Company
Randall	S	Seright	New Mexico Tech
Dongmei		Wang	University of North Dakota

This template is provided to give authors a basic shell for preparing your manuscript for submittal to an SPE meeting or event. Styles have been included (Head1, Head2, Para, FigCaption, etc.) to give you an idea of how your finalized paper will look before it is published by SPE. All manuscripts submitted to SPE will be extracted from this template and tagged into an XML format; SPE's standardized styles and fonts will be used when laying out the final manuscript. Links will be added to your manuscript for references, tables, and equations. Figures and tables should be placed directly after the first paragraph they are mentioned in. The technical content of your paper WILL NOT be changed. Please start your manuscript below.

Abstract

Chemical flooding simulators traditionally assume that polymer retention follows the Langmuir isotherm, while fractional-flow calculations assume concentration-independent retention. Both models predict a delay in propagation of the polymer front (in proportion to the retention value), followed by a rapid rise in produced polymer concentration to the injected level. In contrast, laboratory retention studies for the Milne Point polymer flood (North Slope of Alaska) consistently show virtually no delay in polymer propagation, a rapid rise in produced polymer to 70-90% of the injected concentration, followed by produced concentration gradually approaching the injected value over many pore volumes. From a practical viewpoint, this behavior means that retention causes no significant delay in propagation of the polymer bank (and therefore the oil bank), but the effective viscosity and displacement efficiency are less than originally planned. This paper explores why this polymer "tailing" phenomenon occurs.

During core floods, effluent was analyzed for brine-tracer concentration, viscosity, total organic carbon, and total nitrogen. The latter three items allowed three independent measures of polymer concentration and polymer retention. Experiments were performed with Milne Point core material, oil, brine, and conditions. Mechanistic experiments were also performed with packs of glass beads with controlled levels of various minerals.

In Milne Point cores, the presence of the tailing phenomenon was not sensitive to flow rate, polymer concentration, core heterogeneity, or whether the core was preserved, cleaned of oil, or cleaned and re-saturated with oil, or cleaned, re-saturated and aged with oil. The three independent measures of polymer concentration confirmed that the tailing phenomenon was not an artifact associated with polymer degradation or detection interferences. Tailing was also observed during mechanistic floods using glass-bead packs when sufficient levels of illite or kaolinite were present. This observation was consistent with high levels of illite noted in Milne Point cores. The tailing was not noted during mechanistic floods that contained beads with montmorillonite, chlorite, calcium carbonate, dolomite, siderite, pyrite, or calcium sulfate. A model is proposed to account for the tailing phenomenon.

This work suggests that mineralogy analysis (especially for illite and kaolinite) may reveal whether tailing should be accounted for during simulations of polymer propagation/retention in a given field application.

Introduction

The Milne Point polymer flood is a very successful Department-of-Energy-sponsored pilot project, directed at recovery of ~300 cp oil on the Alaskan North Slope. This project has seen produced water cuts drop from ~70% during waterflooding before the project to less than 10% during polymer injection. Many aspects of this project are documented in Dandekar et al. 2019, 2020, 2021; Ning et al. 2019; Chang et al. 2020; Wang et al. 2020,2022; Dhaliwal et al. 2021; and Zhao et al. 2021. This paper focuses on how polymer retention might impact the Milne Point polymer flood.

In any polymer flood or chemical flood where polymer is used for mobility control, the polymer must propagate deep into the porous rock of the reservoir in order to be effective. Polymer retention (e.g., adsorption, mechanical entrapment) can retard the movement of polymer solutions through the reservoir and thus have an important impact on the efficiency of oil displacement and the economics of a project (Manichand and Seright 2014, Wang et al. 2020). Projections of the impact of polymer retention on a given field project are commonly incorporated into numerical simulations and/or fractional flow calculations (Green and Willhite 2018). Chemical flooding simulators traditionally assume that polymer retention follows the Langmuir isotherm, while fractional-flow calculations usually assume concentration-independent retention. Both models predict a delay in propagation of the polymer front (in proportion to the given retention value), followed by a rapid rise in produced polymer concentration to the injected level. For illustration, the blue curve in **Figure 1** shows polymer propagation predictions using the Langmuir isotherm (in a simulator), while the black-dashed curve shows predictions from an assumption of concentration-independent retention using fractional flow calculations (all assuming 240 $\mu\text{g/g}$ total polymer retention). In contrast, our laboratory retention studies (Wang et al. 2020) for the Milne Point polymer flood (North Slope of Alaska) consistently showed virtually no delay in polymer propagation, a rapid rise in produced polymer to 70-90% of the injected concentration, followed by produced concentration gradually approaching the injected value over many pore volumes. This tailing behavior yields overall retention up to 600 $\mu\text{g/g}$, even though most polymer is not delayed. From a practical viewpoint, this behavior means that retention causes no significant delay in propagation of the polymer bank (and therefore the oil bank), but the effective viscosity and displacement efficiency are less than originally planned. This paper explores why this polymer “tailing” phenomenon occurs.

Detailed aspects of polymer retention were covered during previous reviews (Manichand and Seright 2014; Zhang and Seright 2014; Seright 2017; Wever et al. 2018; Green and Willhite 2018; Guetni et al. 2019; Ferreira and Moreno 2020; Wang et al. 2020; Sugar et al. 2021). However, only Wang et al. 2020 mentioned the tailing phenomenon. Perhaps this phenomenon was not reported previously for fear that the effect might have been an experimental artifact associated with the polymer retention method used. However, in Wang et al. (2020) (and again in this work), three different polymer retention methods were used simultaneously to demonstrate that the tailing phenomenon was a real effect. In addition to the tailing phenomenon, Wang et al. noted that inaccessible pore volume was negligible in Milne Point cores. They also found no evidence of chromatographic separation of HPAM molecular weights during dynamic retention experiments—the intrinsic viscosity of the first polymer produced from a core was (within experimental error) the same as that produced many pore volumes (PV) later.

In this paper, multiple types of laboratory measurements were used to assess HPAM polymer retention. Core floods were used to dynamically determine polymer retention in different Milne Point Schrader Bluff sands, with extensive permeability, grain size distribution, XRD, and XRF characterizations. During all experiments, the effluent was analyzed for brine-tracer concentration, viscosity, total organic carbon, and total nitrogen. The latter three items allowed three independent measures of polymer concentration and polymer retention. Experiments were performed with Milne Point core material, oil, brine, and conditions. Mechanistic experiments were also performed using packs of glass beads with controlled levels of various minerals, including illite, kaolinite, montmorillonite, chlorite, calcium carbonate, dolomite, siderite, pyrite, and calcium sulfate. At the end, a model is proposed to account for the tailing phenomenon.

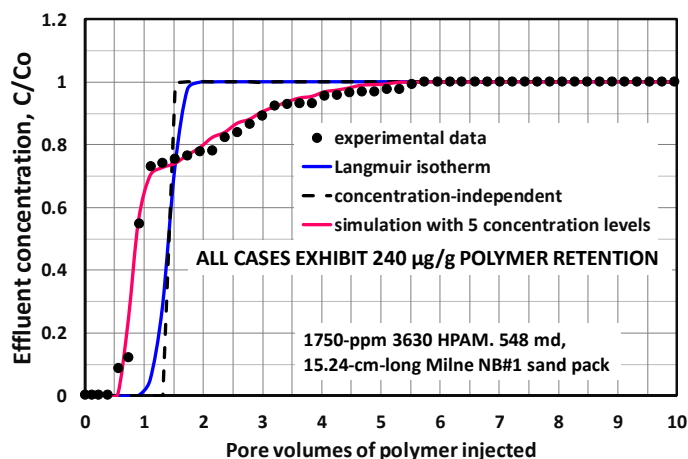


Figure 1—Tailing phenomenon during a polymer retention study versus model predictions.

Materials and Methods

The Brine, Polymers and Polymer Solutions.

The synthetic brine in this work was called Milne Point injection water, which contained 2435-ppm total dissolved solids (not including water of hydration)—consisting of 2173-ppm NaCl, 8-ppm KCl, 357-ppm CaCl₂·2H₂O, and 73-ppm MgCl₂·6H₂O. The calcium and magnesium salts were added as hydrates. This brine was passed through 0.45 µm Millipore filters before further use.

For most of this work, several powder-form partially hydrolyzed polyacrylamides (HPAM) were used: SNF Flopaam 3630S™ (Lot GJ1201, received from the Milne Point field application September 26, 2018), SNF Flopaam 3430S™, SNF Flopaam 3130S™, and Flodrill TS705™. The degree of hydrolysis was 30% for these polymers. In one experiment, Ciba Alcoflood 254S™ was used, which had a 10% degree of hydrolysis. The third column of **Table 1** lists manufacture-stated molecular-weight (Mw) ranges (based on intrinsic viscosity). We made our own measurements of intrinsic viscosity and Mw in the Milne Point injection water, using the methods of Jouenne and Levache (2020). These Mw values are listed in the fourth column, while the fifth column lists C^* values—the critical polymer overlap concentration. Below this concentration, polymer molecules generally float free and un-entangled in solution. Above this concentration, the polymer molecules are entangled with others.

Polymer solutions were prepared by sprinkling polymer powder (over the course of four minutes) onto the brine vortex created by an overhead stirrer (IKA RW-200) at 300 rpm with a four-blade propeller. After initial mixing for several hours at high rate, the stir rate was reduced to ~100 rpm for at least one day. Polymer solutions were confirmed to be homogeneous by the absence of any lumps within a thin layer as the fluid flowed over a beaker lip when poured from one beaker to another. As in the field application, our target polymer solution viscosity was 45 cp (at 7.3 s⁻¹ 25°C). For consistency in many studies, we fixed concentrations at 1750-ppm Flopaam 3630S and 2000-ppm Flopaam 3430S.

Table 1—Mw and C^* parameters for HPAM polymers.

Polymer	Anionicity, %	Manufacturer-stated Mw million g/mol	Measured Mw, million g/mol	C^* , ppm
Flopaam 3630S	30	17 – 19	18**	200
Flopaam 3430S	30	10 – 12	11	300
Flopaam 3130S	30	3 – 5	2.7	850
Flodrill TS705	30	--	0.3	4500
Alcoflood 254S	10	0.25 - 0.5	0.1	10000

** This case was used as a starting basis for the calculations and comparison.

The Sands.

The Schrader Bluff sands of the Milne Point polymer flood were the NB sand and the OA sand. The current polymer pilot is flooding NB sands, but OA sands are of high interest for expansion of the polymer

flood. Our experiments used NB sands (provided by Hilcorp) from two different wells (located 3000 ft apart and at slightly different depths). We labeled NB sands from 3908 ft of the Pesado well as “NB#1”; and NB sands from 3757 ft of the Liviano well as “NB#3”. The OA sand used in this work was from 4067 ft of the Pesado well. The sands are fairly similar in elemental composition, except the OA sand contains 5-7 times as much calcium, 30% more iron, and 30-100% more magnesium, and 70-90% less sulfur than the NB sands. The NB#3 sand had 4-5 times as much sulfur as the NB#1 sand. The clay contents of the various sands were similar, with the NB#3 sand containing slightly less than the others. The OA sand contained noticeably more dolomite and feldspar (albite and orthoclase) than the NB sands. Grain-size distributions were obtained for the sands and materials used to make synthetic sand packs. These distributions were obtained using a laser-diffraction method (Malvern Mastersizer 3000™ with Hydro EV™ dispersing unit), which provides volume-based measurements.

Sand Pack Preparation.

Our packing procedures are described in Wang et al. (2020). Typically for the current work, we used biaxial Temco Hassler core holders. These were 2.54-cm diameter, and usually either 15.24-cm or 30.48-cm in length. To fine-tune the desired pack permeability, the confining pressure (i.e., overburden pressure) was varied (between 100 and 1750 psi). However, 500 psi confining pressure was most commonly used, unless stated otherwise. GE Druck DPI 104™ pressure transducers were used—either 1000-psi transducers with 0.1 psi readout or 300-psi transducers with 0.01 psi readout. Four ISCO (Model 500D or 1000D™) pumps were used during a typical experiment—one each for brine, polymer solution, oil, and confining pressure.

The condition of the sand varied. In some cases, the sand was used as received (“native state”). Other times, the sand was washed/extracted with toluene and methanol and dried before use. In some cases, the sands were saturated only with brine before use. In other cases, the sand packs were flooded with fresh Milne Point oil (viscosity ~ 111 cp at 25°C) to connate water saturation, followed by flooding with at least 150 PV of brine to drive the sand pack to residual oil saturation. Preserved cores were also used.

Flood Sequence and Polymer and Tracer Detection.

After pack saturation, characterization, and stabilization of brine injection at a low rate (typically, 1.86 or 3.7 ft/d darcy velocity), 5-13 PV of polymer solution were injected at a fixed rate, while monitoring pressure drops across the pack or pack sections.

Effluent from packs was analyzed by several methods. Routinely, we monitored a water tracer (20-ppm potassium iodide) using a Genesys 2™ spectrophotometer at a wavelength of 230 nm. Effluent polymer concentration was monitored by three methods: total organic carbon, total nitrogen, and viscosity. For total organic carbon, a Shimadzu TOC-L™ was used. We recognize that this measurement might be influenced by the presence of any oil. Total nitrogen was measured using chemiluminescence with a Shimadzu TNM-L™ unit. Viscosity was measured at 7.3 s⁻¹ (25°C) using proRheo LS-300™ and/or Vilastic VE™ rheometers. The previous measurements were made at 3-4 cm³ increments for each effluent sample.

Figure 2 illustrates the results during 10 PV of polymer injection (2000-ppm Flopaam 3430S) for a 15.24-cm-long pack with 232-md native-state OA sand with 500-psi confining pressure. In Figure 2, all values are reported relative to the injected values. The dashed blue curve shows the tracer (KI) breakout. The black and green curves show breakout of the polymer, as judged by carbon content and nitrogen content, respectively. The solid red curve plots effluent produced polymer concentrations that were based on viscosities (using a relation between viscosity and concentration that was reported in Wang et al. 2020).

The difference in area between the tracer (dashed blue) curve and a given polymer curve in Figure 2 can be used to calculate polymer retention (if one assumes that inaccessible pore volume is zero). Specifically, Eq. 1 (from Manichand and Seright, 2014) provides a means for the calculations:

$$R_{pret} = \{[\sum [(C_p/C_{po} * \Delta PV) - (C_t/C_{to} * \Delta PV)]] + IAPV\} * C_{po} * PV / M_{rock} \dots \dots \dots (1)$$

where R_{pret} is polymer retention, C_p is effluent polymer concentration, C_{po} is injected polymer concentration, C_t is effluent tracer concentration, C_{to} is injected tracer concentration, PV is the volume in one pore volume, ΔPV is pore-volume increment, and M_{rock} is the rock mass in the sand pack.

In Figure 2, polymer retention values were 236 $\mu\text{g/g}$ based on effluent nitrogen, 156 $\mu\text{g/g}$ based on effluent carbon, and 204 $\mu\text{g/g}$ using viscosity-based concentration. The nitrogen-based calculation provides the most reliable answer because the carbon-based method could be influenced by any carbon contamination (e.g., residual oil) and polymer degradation could affect the viscosity-based method. Consequently, all subsequent retention values reported in this paper are based on nitrogen detection.

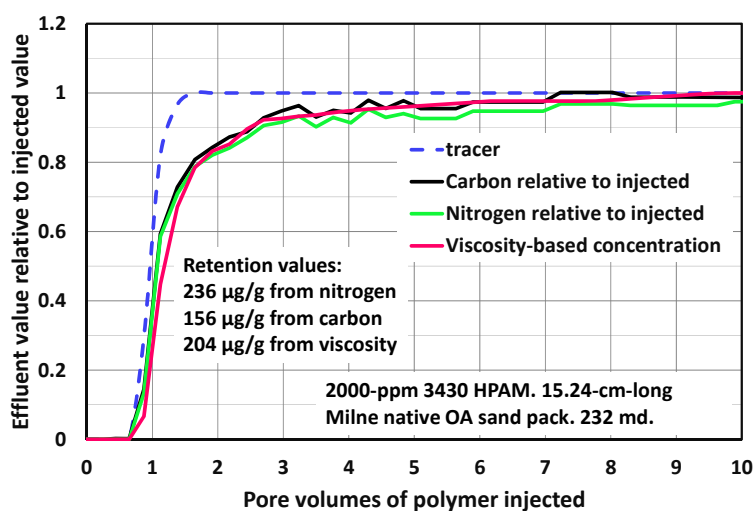


Figure 2—Effluent composition during polymer injection (232-md native OA sand).

Results in Milne Point Core Material

Effect of Fluid Velocity.

It seemed conceivable that the tailing phenomenon is related to diffusion—so that the magnitude of the tail might be sensitive to velocity at which the experiment was performed. To test this idea, separate retention experiments were performed at different rates, ranging from 0.31 to 3.7 ft/d (darcy velocity). These experiments used 1750-ppm Flopaam 3630S in 15.24-cm-long sand packs of native NB#1 sand that had permeability (to brine) ranging from 203 to 287 md. **Figure 3** demonstrates that rate did not significantly affect the shape of the polymer breakout curves. For the three cases, the effluent concentration rapidly rose to ~70% of the injected value (at 1.5 PV) and then tailed up to ~90% of the injected value after 10 PV. Overall retention values calculated at 10 PV ranged from 339 to 482 $\mu\text{g/g}$ —with most of the retention associated with the tail. Of the total retention values listed, 209–305 $\mu\text{g/g}$ was associated with the tailing phenomenon (i.e., materializing after 2 PV of polymer injection). Considering the variations seen in Figure 3, we do not consider these values to be significantly different. Thus, the tailing phenomenon did not appear to be sensitive to fluid velocity.

Effect of Particle Size.

A second thought was that perhaps the tailing phenomenon might depend on the particle size or size distribution of the sand. To test this concept, a portion of NB#1 sand was sieved to produce two sand fractions: one fraction that was between 20 and 35 mesh (841–500 μm) and the other fraction that passed through a 35-mesh screen (<500 μm). **Figure 4** shows the particle size distributions of the two fractions, as measured using a Malvern Mastersizer™ 3000 particle size analyzer. The median particle sizes [Dv(50)] for the two sand fractions were 692 μm and 231 μm , respectively, while the main peaks occurred

at 666 μm and 211 μm , respectively. **Figure 5** compares results from two retention experiments using these two sand fractions, conducted under the same conditions. Retention values (determined at 10 PV polymer throughput) ranged from 337 to 461 $\mu\text{g/g}$, and the two effluent curves were quite similar. Thus, the tailing phenomenon did not appear to be sensitive to sand particle size.

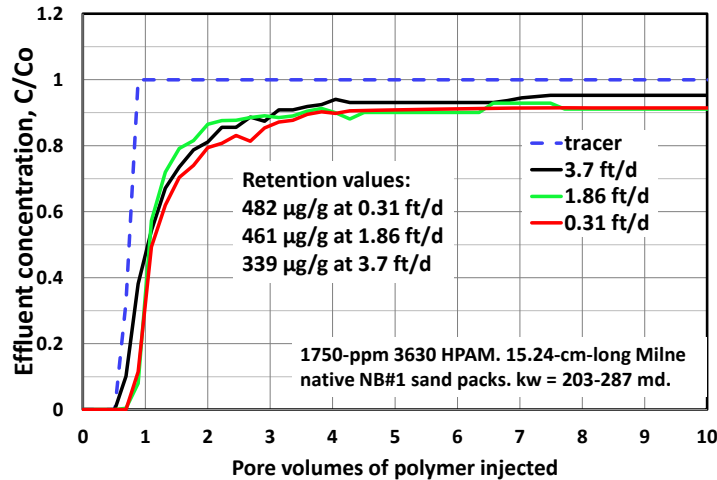


Figure 3—Effect of rate on tailing phenomenon in native NB#1 sand packs.

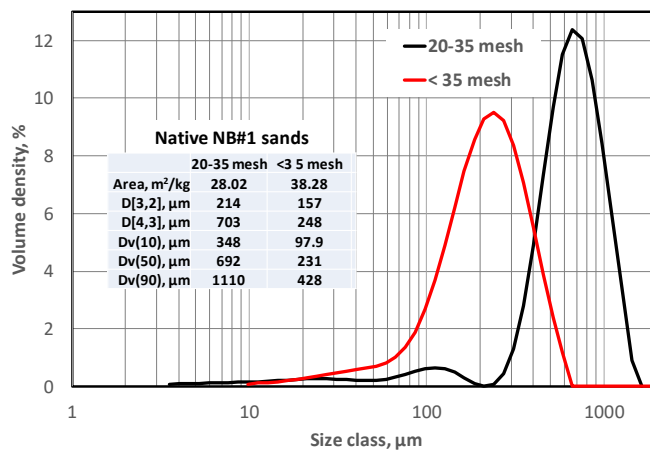


Figure 4—Particle size distributions for sieved NB#1 sands.

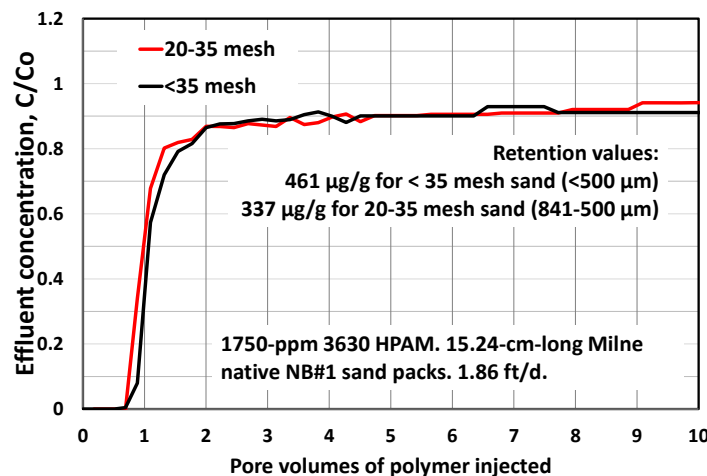


Figure 5—Effect of particle size on tailing phenomenon in native NB#1 sand packs.

Effect of Sand Source, Polymer Concentration, and Molecular Weight.

Another question was whether the tailing phenomenon depends on polymer concentration or molecular weight used for the retention study. This idea was tested by performing retention studies in native OA sand packs, with concentrations of Flopaam 3630S ranging from 600 to 1750 ppm. The results are shown in **Figure 6**. The tailing phenomenon observed was quite similar to that observed in sand packs using NB#1 sand. Thus, the tailing phenomenon was seen in sand from two different Schrader Bluff sands (OA and NB) from the same well. Further, the shapes of the polymer breakout curves were very similar, regardless of polymer concentration (between 600- and 1750-ppm Flopaam 3630S). The retention values for the three cases varied from 66 to 205 $\mu\text{g/g}$, primarily because polymer concentration weighs heavily in the retention calculation (see Eq. 1).

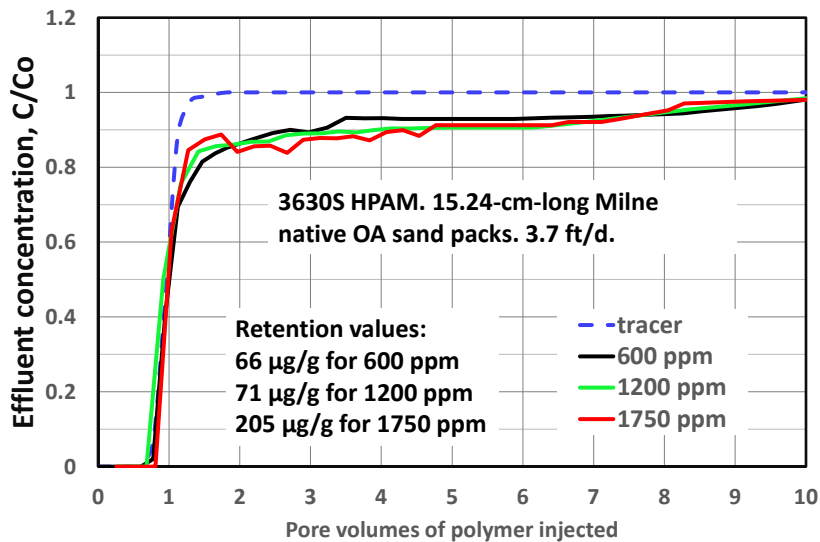


Figure 6—Effect of polymer concentration on tailing phenomenon in native OA sand packs.

Figure 7 shows that a similar tailing effect occurred (in native OA sand) for 2000-ppm Flopaam 3430S—a solution providing about the same polymer viscosity as 1750-ppm 3630S, but using a lower-molecular-weight HPAM (11 million g/mol versus 18 million g/mol). Polymer retention was about the same for the two cases (i.e., 236 $\mu\text{g/g}$ for 2000-ppm 3430S versus 205 $\mu\text{g/g}$ for 1750-ppm 3630S).

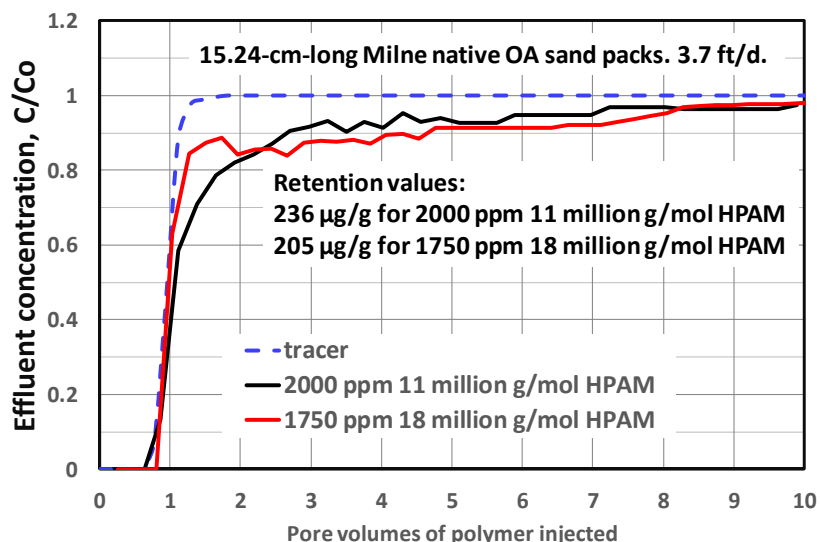


Figure 7—Effect of polymer Mw on tailing phenomenon in native OA sand packs.

Effect of Core Preservation State.

A number of experiments were performed to determine whether the tailing phenomenon might be an artifact associated with how the core was preserved or restored. **Figure 8** shows that the tailing phenomenon was observed for a 6.7-cm-long preserved core from the Schrader Bluff NB sand. We also found tailing during retention studies in preserved OA cores. In previous work (Wang et al. 2020), tailing was noted in (1) native-state NB and OA sands, (2) cleaned (by extraction with toluene and methanol) NB and OA sands, (3) NB and OA sands that were cleaned and then re-saturated with fresh Milne Point oil, and (4) cleaned, re-saturated, and aged (at 60°C) NB cores. Combining this current work with the previous work, we note that the tailing phenomenon persisted in cores with different lengths (5.08-60 cm), permeabilities (50-6108 md), and confinement pressures (100-1750 psi).

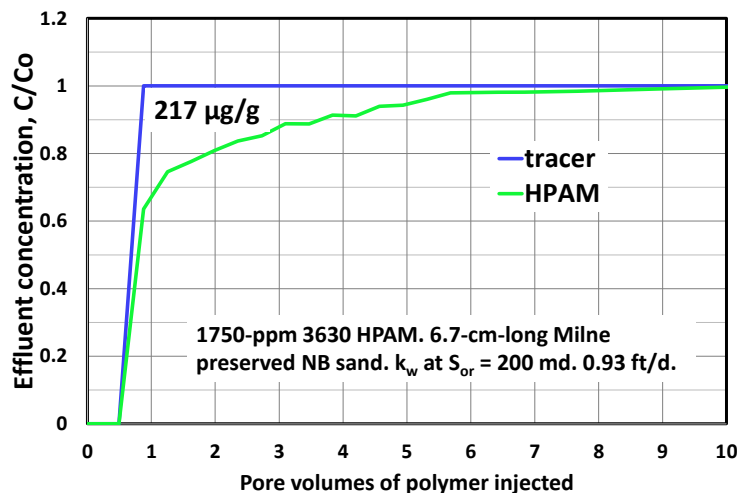


Figure 8—Tailing phenomenon in a preserved NB sand pack.

Studies in Bead Packs with Known Additions of Selected Minerals

Particle Size Distributions.

Although the tailing phenomenon persists throughout these studies, we cannot yet identify a reason for its existence. Consequently, we performed a number of retention studies in “synthetic” packs of known composition—to examine how the tailing phenomenon depends on mineral composition. Our base-case for these studies involved injection of 1750-ppm Flopaam 3630S into a 7-darcy pack of 200- μ m glass beads (of very narrow size distribution). **Figure 9** shows the particle size distributions for these beads and for three Schrader Bluff sands. The mean particle size [$D_v(50)$] for the beads (212 μ m) was reasonably close to that for the NB#1 sand (166 μ m). For the beads and each of the sands, various standard characterization parameters are listed in the table within Figure 9. These parameters are defined in the Nomenclature.

Figure A-1 in **Appendix A** plots particle size distributions for four clays (illite, chlorite, kaolinite, and montmorillonite) that were used in this study. XRD studies (Jones 2010; Rose et al. 2011; Wang et al. 2020) indicated that illite was commonly present in Milne Point core material—although a wide range of illite compositions were reported (1-21%). **Figure A-2** plots size distributions for five other materials that were used in this study—limestone [CaCO_3], dolomite [$\text{CaMg}(\text{CO}_3)_2$], siderite [FeCO_3], pyrite (FeS_2), and CaSO_4 . All distributions in Figures A-1 and A-2 were very broad, usually with multiple peaks.

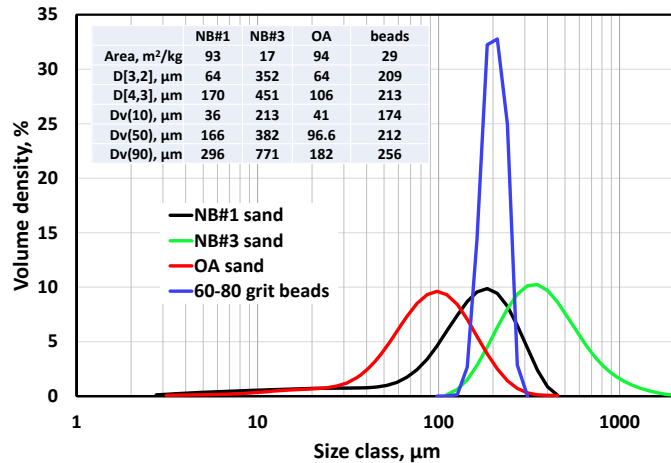


Figure 9—Particle size distributions for glass beads versus three sands.

In a 7-darcy bead pack (with no added minerals), polymer retention was zero and no tailing occurred. **Figure 10** shows that the tailing phenomenon occurred to various extents with bead packs that contained 9% of the clays (kaolin, illite, and chlorite), with the remainder of the pack being the 200-μm beads. The 9% kaolin pack had a permeability of 192-md and exhibited retention of 76 μg/g. The 9% illite pack had a permeability of 4646-md and exhibited a retention of 125 μg/g. The 9% chlorite pack had a permeability of 2858-md and exhibited a retention of 13 μg/g. The retention and tailing for chlorite were not significant—perhaps because the particles of chlorite were larger than those of the other clays (blue curve in Figure A-1).

In contrast to illite and kaolin, a 938-md bead pack with 9% limestone exhibited polymer retention of 186 μg/g but showed no sign of tailing (dashed pink curve in Figure 10). Additional bead pack studies with 5% and 13% limestone also showed no tailing, with retention values of 48 μg/g and 162 μg/g, respectively. No tailing phenomena were seen in bead packs with (1) 9% montmorillonite—which provided a 135-md pack and exhibited no retention. (2) 9% dolomite—which provided a 2456-md pack and exhibited 52 μg/g retention, (3) 9% siderite—which provided a 1586-md pack and exhibited 49 μg/g retention, (5) 9% pyrite—which provided a 5760-md pack and exhibited 4 μg/g retention, and (6) 2% CaSO₄—which provided a 700-md pack and exhibited no polymer retention,

Thus, our results suggest that illite and kaolinite were the only minerals tested so far that exhibit the tailing phenomenon and might be the source of the tailing phenomenon in Milne Point cores. It is interesting that retention and tailing were not significant for the clays, montmorillonite and chlorite and also for pyrite. No correlation is evident with permeability or grain size distribution.

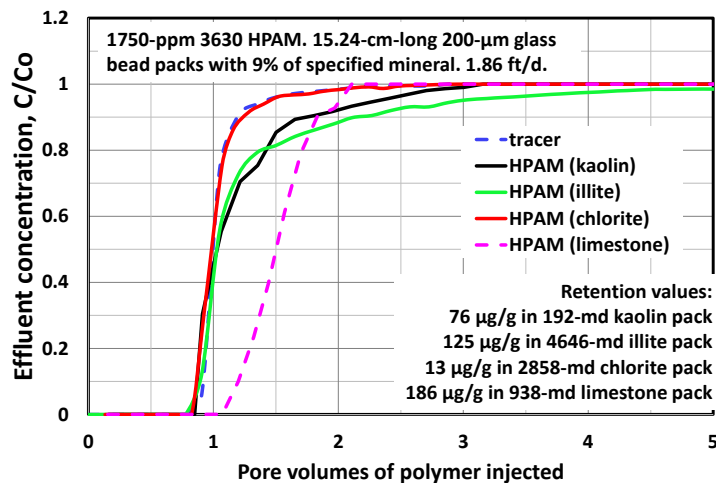


Figure 10—Tailing phenomenon in bead packs with various minerals.

Retention Studies in Bead Packs with Illite

Additional studies were performed with bead packs that contained illite, since (1) XRD studies indicated that illite is the dominant clay present in Milne Point core material and (2) illite is one of two minerals that definitively showed the tailing phenomenon.

Effect of Particle Size.

To test how particle size affects polymer retention and tailing, we performed retention tests using three illite samples. The first sample was illite with the particle size distribution shown by the red curve in **Figure 11**—where the median particle size was 330 μm . For the second and third illite samples, the first sample was sieved to produce a fraction that passed through 100 mesh (149 μm) and another fraction that passed through 20 mesh (841 μm) but was retained by 100 mesh. The second sample (through 100 mesh) had the particle size distribution shown by the green curve in Figure 11—where the median particle size was 29.3 μm . The third sample (between 20 and 100 mesh) had the particle size distribution shown by the black curve in Figure 11—where the median particle size was 509 μm . Note from the black curve that a small quantity of small particles was retained on the 100-mesh screen. The peaks for the small particles (at 0.6 μm and 5.2 μm) in the black curve were at least 20 times smaller than for the large peak (at 586 μm). The green curve had no particles larger than 300 μm . For comparison, the blue curve in Figure 11 shows the particle size distribution for the 200- μm glass beads.

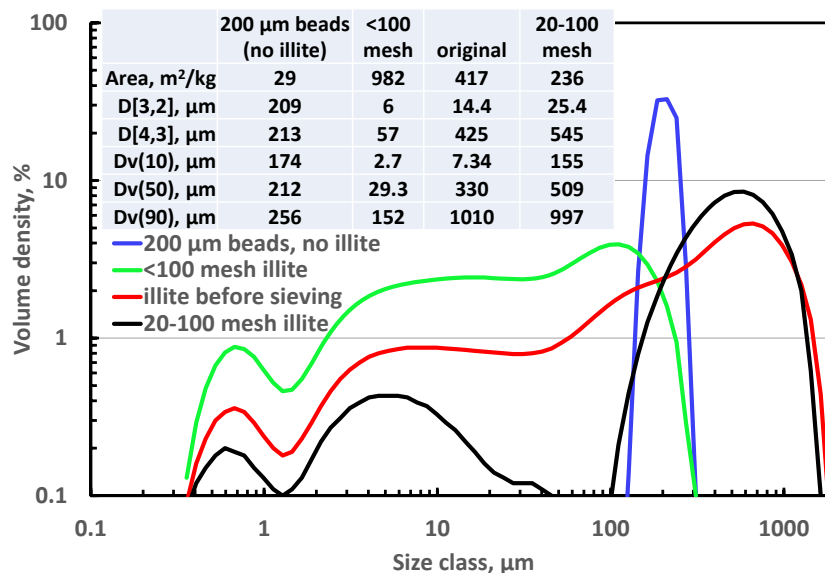


Figure 11—Illite particle size distributions before and after sieving.

Each of these three illite samples (from the same original source) was mixed with 200- μm glass beads—to make 9% illite in each of three packs. **Figure 12** shows the results of the retention tests using the three illite samples, along with results using only the 200- μm beads (with no illite). Note that the three illite samples exhibited very similar tailing phenomena and retention values (117-125 $\mu\text{g}/\text{g}$). Close examination indicates that retention and tailing were very slightly greater as particle size decreased. However, for the most part, retention and tailing were apparently not sensitive to particle size or permeability (from 1408 to 6107 md). This finding is consistent with that observed for polymer retention in the Milne Point cores (Figure 5).

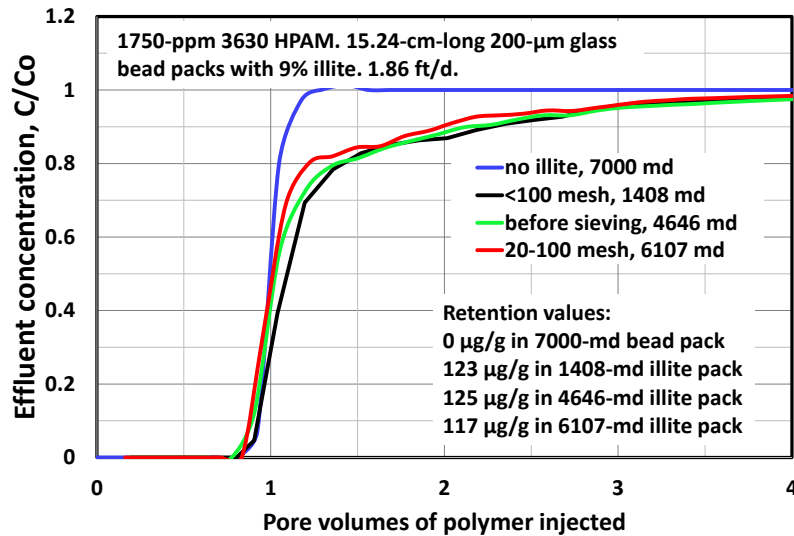


Figure 12—Tailing phenomenon in 9% illite before versus after sieving.

Effect of Flooding Rate.

To test whether the tailing phenomenon is sensitive to flooding rate, two additional experiments were performed (using the illite that passed through 100 mesh) at 0.31 ft/d and 12.4 ft/d, respectively. **Figure 13** reveals that retention and tailing became modestly greater as rate was decreased from 12.4 to 0.31 ft/d. The effect was most evident between 1 and 2 PV. This relative insensitivity to rate for retention in illite was consistent with that observed for retention in the Milne Point cores (Figure 3).

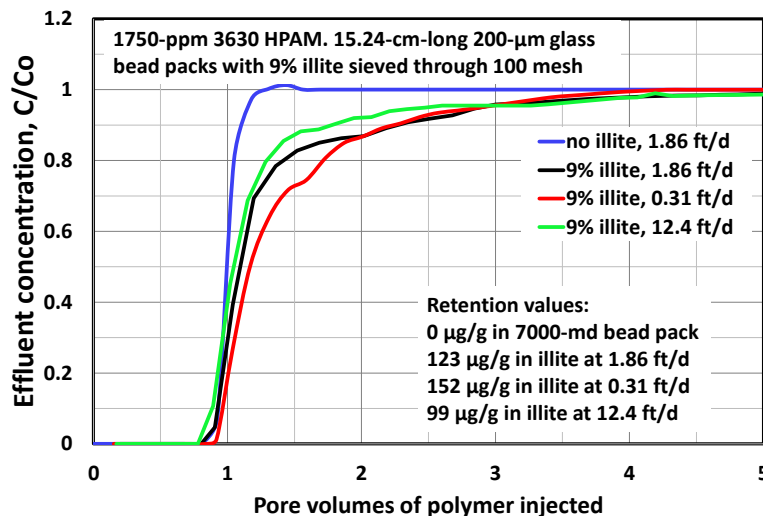


Figure 13—Tailing phenomenon in 9% illite versus flooding rate.

Effect of Polymer Molecular Weight, Concentration, and Anionicity.

Figures 6 and 7 suggested that the tailing was not sensitive to HPAM concentration (between 600 and 1750 ppm) or Mw (between 11 and 18 million g/mol) in Milne Point core material. However, we were concerned that greater ranges of concentration and Mw were needed to properly investigate these effects. Consequently, additional retention studies were performed using SNF Flopaam 3130S (Mw~2.7 million g/mol) and SNF Flodrill TS705 (Mw~0.3 million g/mol). All SNF polymer had 30% anionicity (degree of hydrolysis). We also tested Ciba Alcoflood 254S (Mw~0.1 million g/mol, 10% anionicity). The experiments were performed in bead packs with 9% illite (that was sieved through 100 mesh) using 1750-ppm and 200-ppm HPAM.

Comparison of the solid and dashed red and black curves in **Figure 14** reveals qualitatively similar behavior for the 2.7- and 18-million-g/mol polymers—except that the 2.7-million-g/mol HPAM exhibited less than half the retention—especially between 1 and 2.5 PV. Retention values for these cases are listed in **Table 2**.

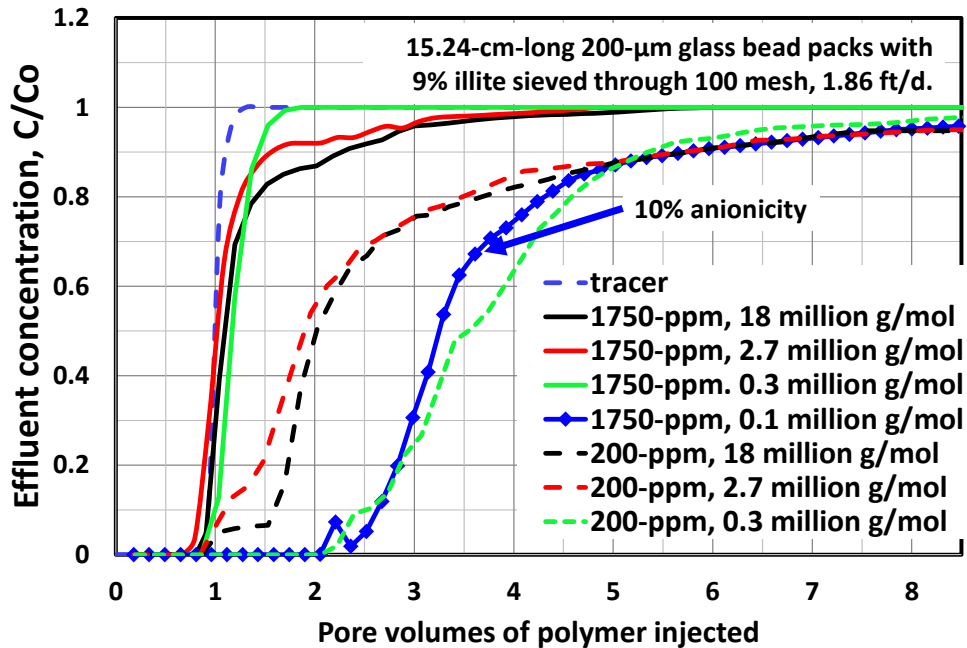


Figure 14—Tailing phenomenon in 9% illite versus HPAM molecular weight and concentration (30% anionicity).

Table 2—Effect of various parameters for HPAM retention on illite (with 200 µm beads)

Mw, 10 ⁶ g/mol	Anionicity, %	HPAM, ppm	Illite, %	Illite sieving	Rate, ft/d	Length, cm	Overall retention, µg/g	Retention, µg/g of illite
18	30	1750	9	<100 mesh	0.31	15.24	152	1672
18	30	1750	9	<100 mesh,	1.86	15.24	123	1353
18	30	1750	9	<100 mesh,	12.4	15.24	99	1089
18	30	200	9	<100 mesh	1.86	15.24	162	1782
2.7	30	1750	9	<100 mesh	1.86	15.24	53	583
2.7	30	200	9	<100 mesh	1.86	15.24	80	880
0.3	30	1750	9	<100 mesh	1.86	15.24	71	781
0.3	30	200	9	<100 mesh	1.86	15.24	102	1122
0.1	10	1750	9	<100 mesh	1.86	15.24	972	10692
18	30	1750	9	no sieving	1.86	15.24	125	1375
18	30	1750	9	20-100 mesh	1.86	15.24	117	1287
18	30	1750	9	20-100 mesh	1.86	30.48	69	759
18	30	1750	9	20-100 mesh	1.86	61.00	100	1100
18	30	1750	4.5	20-100 mesh	1.86	15.24	3	66
18	30	1750	18	20-100 mesh	1.86	15.24	133	732
18	30	1750	36	20-100 mesh	1.86	15.24	209	575

Interestingly, the 0.3-million-g/mol HPAM at 1750-ppm (solid green curve) exhibited no tailing, but a slight delay in initial polymer breakthrough (consistent with the Langmuir isotherm), yielding 71 µg/g retention. In contrast, the blue-diamond curve in Figure 14 shows that the 0.1-million-g/mol polymer (10% anionicity) exhibited a substantial delay in polymer propagation. In this case, no polymer was produced until 2-2.5 PV. The solid red and black curves in Figure 14 showed that the higher-Mw (2.7 and 18 million g/mol) polymers (at 1750 ppm) exhibited no delay in polymer breakthrough. This difference suggests that either the lowest-Mw HPAM (0.1 million g/mol) can penetrate deeper into the illite—leading to very high adsorption/retention (972 µg/g)—or that 10% anionicity causes substantially greater adsorption/retention than 30% anionicity. In contrast, the higher-Mw HPAMs appear largely unable to penetrate into the illite upon initial contact—resulting in significantly lower retention (53 to 123 µg/g).

Note that all (except one: the 0.3-million-g/mol HPAM at 1750-ppm) polymers exhibit substantial tailing after polymer breakthrough (when 9% illite was present). This result suggests that even the lowest-Mw polymer (0.1 g/mol) experiences difficulty in penetrating into the tightest illite pores. For 200-ppm of the 2.7- and 18-million g/mol HPAMs (dashed red and black curves), the retention curves were notably below the solid red and black curves (1750 ppm). The polymer concentration was at or below C^* for the dashed red and black curves and for the blue-diamond and green curves (see Table 1)—suggesting that the polymer more easily penetrates into the illite when the polymer concentration is at or below C^* . However, one could argue that the solid green curve (0.3-million g/mol at 1750 ppm) might be an exception to this rule. Figure 14 and Table 2 suggest a complicated relation between polymer retention on illite and polymer Mw, concentration, and anionicity.

Effect of Illite Content.

To test how the tailing phenomenon depends on illite composition in the pack, additional experiments were performed (using the illite that passed through 20 mesh but was retained by 100 mesh). The illite content ranged from 4.5% to 36%, corresponding to pack permeabilities that ranged from 1730 to 6527 md. **Figure 15** shows the results. Very little retention (3 $\mu\text{g/g}$) was seen with 4.5% illite. The dashed black curve in Figure 15 was quite similar to that for the KI tracer curve (not shown) for the 4.5%-illite case, and tailing was not particularly evident. In contrast, retention increased from 117 $\mu\text{g/g}$ to 209 $\mu\text{g/g}$ as illite content rose from 9% to 36%. The level of tailing became more pronounced also. In Figure 15, the produced polymer concentrations departed from the KI-tracer curves at $\sim 80\%$ (of injected concentration) for 9% illite (green curve), $\sim 70\%$ for 18% illite (red curve), and $\sim 50\%$ for 36% illite (solid black curve). The produced polymer concentrations reached the injected values at ~ 4 PV for 9% illite, ~ 5 PV for 18% illite, and ~ 10 PV for 36% illite. These results suggest that the level of contact of polymer with illite was important. All cores visually appeared to have the illite uniformly distributed throughout the core—as judged by the color, texture and core integrity. Of course, the illite could have experienced segregation on a sub-visual level. However, if the illite was macroscopically segregated, the KI tracer breakout curves should have reflected this—via a noticeable tail in the KI breakout curves. In contrast, all KI tracer breakout curves for these cases were quite sharp (like the blue curves in Figures 2 and 3)—indicating homogeneous cores. Further, as shown in **Figure 16**, a plot of log of permeability versus porosity (red data points and line) follows a consistent relation with changing illite content. If substantial segregation occurred for the beads and illite, one would have expected a substantial deviation for the plot in Figure 16, as suggested by the dashed blue curve (which was calculated assuming Darcy's law for flow in parallel for totally segregated material).

We also performed an experiment that contained only 20-100-mesh illite (i.e., no glass beads). When subjected to 500 psi confining pressure, permeability to brine was only 0.4 md. Due to the low permeability, polymer injection was not attempted. Instead, we dried the pack and re-determined the particle size distribution (red curve in **Figure A-3** in Appendix A)—to see if the process of compression (to 500 psi) affected particle size. Figure A-3 illustrates that the compression process did indeed alter the illite size distribution—by significantly increasing the fraction of smaller illite particles. The black curve in Figure A-3 shows the original particle size distribution for illite, while the green curve shows the size distribution after sieving between 20 mesh (841 μm) and 100 mesh (149 μm). (This sieved material was used for the experiments in Figures 12, 15 and 17.) Comparison with the red curve in Figure A-3 indicates that the compression process produced small particles so that the low end of the size distribution (below 100 μm) matched that associated with the original un-sieved illite (i.e., the black curve).

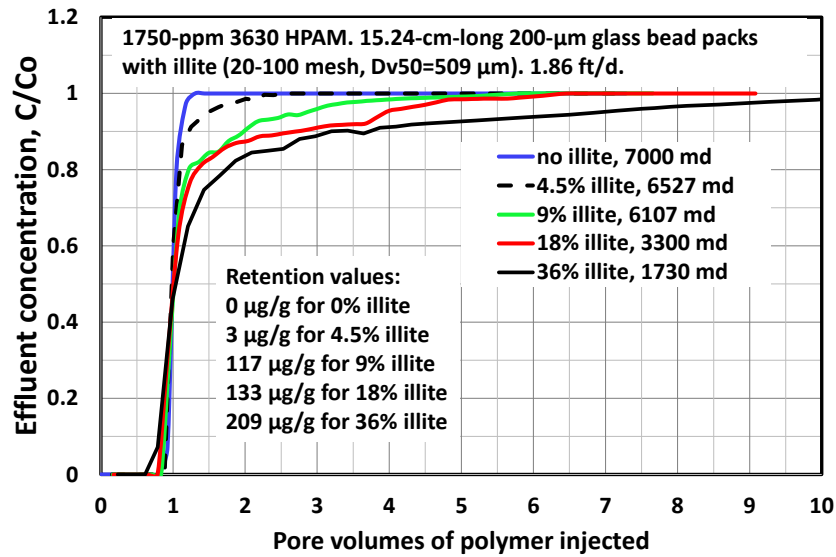


Figure 15—Tailing phenomenon in 20-100-mesh illite versus illite content in bead pack.

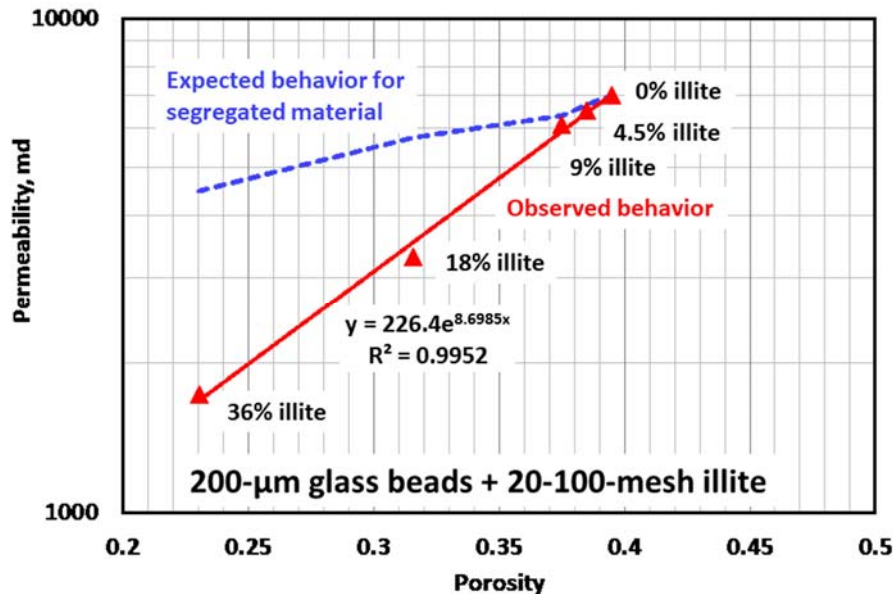


Figure 16—Permeability-porosity relation versus illite content.

Effect of Pack Length.

Using packs that contained 9% illite (20-100 mesh), Figure 17 shows that the tailing phenomenon persisted for pack lengths from 15.24 to 61 cm. Although some variation was observed, the nature of the tailing was similar over this range of lengths—with total retention values from 69 to 117 $\mu\text{g/g}$. If the tailing was caused by channeling of polymer through a pack (because of heterogeneity or uneven illite distribution along the pack), one would have expected the tailing to be mitigated as pack length increased. So, the behavior in Figure 17 is consistent with our other observations indicating that the packs were all reasonably homogeneous—and the tailing was not due to uneven contact with illite within the packs.

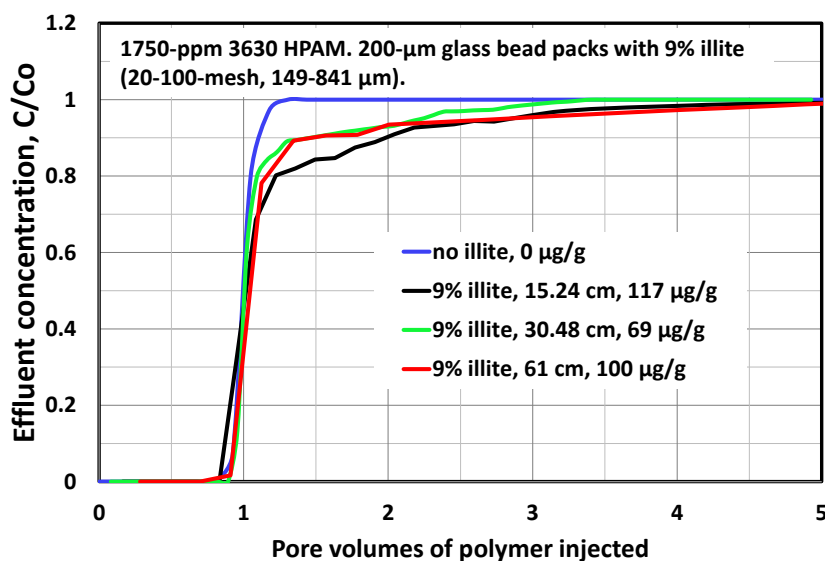


Figure 17—Tailing phenomenon in 20-100-mesh illite versus pack length.

Discussion

Heterogeneity/Multiple Paths.

A tailing phenomenon is often seen when a water tracer is continuously injected into a heterogeneous core (Perkins and Johnston 1963; Home and Rodriguez 1983; Yang et al. 2021). In a homogeneous core or sand pack, the pathways through the porous medium are randomized, so no particular pathway has much preference over another. Consequently, the tracer arrives at the end of the core and rises to match the injected concentration in a fairly sharp manner—like the blue curves in Figures 2, 3, 6, 7, 8, 10 and 14. In contrast, in a heterogeneous porous medium, tracer will arrive in the effluent early by traveling through the most direct and permeable pathway. After breakthrough, tracer from less-permeable pathways will arrive in the effluent at different times—thus giving the appearance of a concentration tail. Since our water tracer curves always gave sharp breakout curves, our cores and sand packs were homogeneous. Also, for the bead packs, the coloration and shading given by various additives suggested that the packs had no obvious heterogeneity (e.g., separation between the 200- μm beads and the added mineral). Nevertheless, it is possible that the polymer saw heterogeneity as it propagated through the core, even though the tracer did not. Inaccessible pore volume (IAPV) is such a phenomenon (Dawson and Lantz 1972; Manichand and Seright 2014; Wang et al. 2020). It is possible that the KI tracer can freely flow through the illite but the high molecular-weight polymer has limited access.

Surface Area/Particle Size.

Electron micrographs of illite (Keller et al. 1986) show the surfaces to be quite rough. Polymer adsorption is expected to depend on the surface area of the adsorbing mineral. For a fixed weight of mineral, small particles will have a larger surface area than large particles. Consequently, one would expect polymer retention should be noticeably higher for packs with small particles than with large particles. In contrast, this concept does not receive much support from Figures 4 and 5 (for Milne Point core material) or from Figures 11 and 12 (for packs with 9% illite). Whatever is causing the tailing phenomenon seems to be fairly insensitive to particle size. However, as suggested by Figure A-3, compression of the clay (e.g., to 500 psi) may have renormalized the illite size distribution to more closely match the original, un-sieved clay. In that case, perhaps all our illite cases that were compressed actually had similar distributions of small illite particles. Also, the particle-size measurements were made under conditions where the particles were well-dispersed so that all grains had minimum contact with other particles. The extensive grain contact in compacted cores would substantially reduce the surface area that could contact the polymer.

Retention per g of Illite.

For much of the above data for bead packs with illite, Table 2 summarizes the results and (in the last column) expresses HPAM retention as μg per gram of illite. Previous calculations (summarized in the eighth column) included all solids (i.e., glass beads plus mineral) in the denominator of the retention calculation. If the results are excluded for the 4.5%-illite case and the polymer with 10% anionicity, HPAM retention averaged 1100 μg of polymer per gram of illite—with variations extending from 575 to 1782 $\mu\text{g/g}$. Thus, it appears that for 9% illite and above, HPAM (with anionicity=30%) retention (after many PV of polymer injection) is roughly 1100 $\mu\text{g/g}$ of illite, regardless of other conditions. However, from the last column of Table 2, we note that the average retention on illite that was sieved through 100 mesh ($<149\ \mu\text{m}$) was generally higher than that for 20-100-mesh (149-841 μm) illite. This observation is consistent with the idea that smaller particles have a greater surface area and therefore should exhibit higher HPAM retention.

Proposed model.

In formulating a model for the retention tailing phenomenon, the model must account for the experimental observations mentioned previously. One can conceive of multiple mechanisms. Some mechanisms that could not adequately explain our experimental observations (e.g., polymer imbibition, flocculation) are discussed in **Appendix B**. This section will focus on the most applicable mechanism that we have examined to date.

Much of the data (for HPAM with $M_w=18$ -million g/mol, 30% anionicity in packs with 9% illite) could be fitted using an “exposure parameter”, Lp , that is defined in Eq. 2:

$$Lp = (t - t_{bt}) u C^{0.5} \dots\dots\dots (2)$$

where, t is time since the start of polymer injection (seconds), t_{bt} is the time of first polymer arrival at the end of the core (seconds), u is darcy velocity (cm/s), and C is injected polymer concentration (weight fraction). The units for Lp are $\text{cm} \cdot (\text{wt. fraction})^{0.5}$. The effluent polymer concentration, relative to the injected value, C/C_o , was predicted quite well using Eq. 3.

$$C/C_o = 1 - 0.7 e^{-Lp/0.03} - 0.3 e^{-Lp/0.25} \dots\dots\dots (3)$$

The solid red curve in Figure 18 reveals that this model described the observed behavior quite well for HPAM concentrations from 200 to 1750 ppm, darcy velocities from 0.31 to 12.4 ft/d, pack lengths from 15.24 to 61 cm, and independent of illite particle size.

To rationalize this model, we note that polymer retention depends on the total time ($t - t_{bt}$) of polymer exposure to illite. This time difference is multiplied by the injection rate, u , to reflect that slow rates cause longer exposure times for a given fluid element. This product is then multiplied by the square root of polymer concentration. One would expect that lower HPAM concentrations would show reduced reaction rates. However, the cause of the dependence on the square root of concentration is less obvious.

In Eq. 3, the two exponential terms suggest that two exposure-dependent processes occurred at the same time. The middle term reveals that $\sim 70\%$ of the concentration change was due to a relatively short process (with an exposure constant of 0.03), while the third term indicates that $\sim 30\%$ of the concentration change was ascribed to the longer process (with an exposure constant of 0.25). Conceivably, the short process could be HPAM adsorption onto the outer (most accessible) surface of the illite, while the longer process could be associated with HPAM penetrating more deeply into the rough illite.

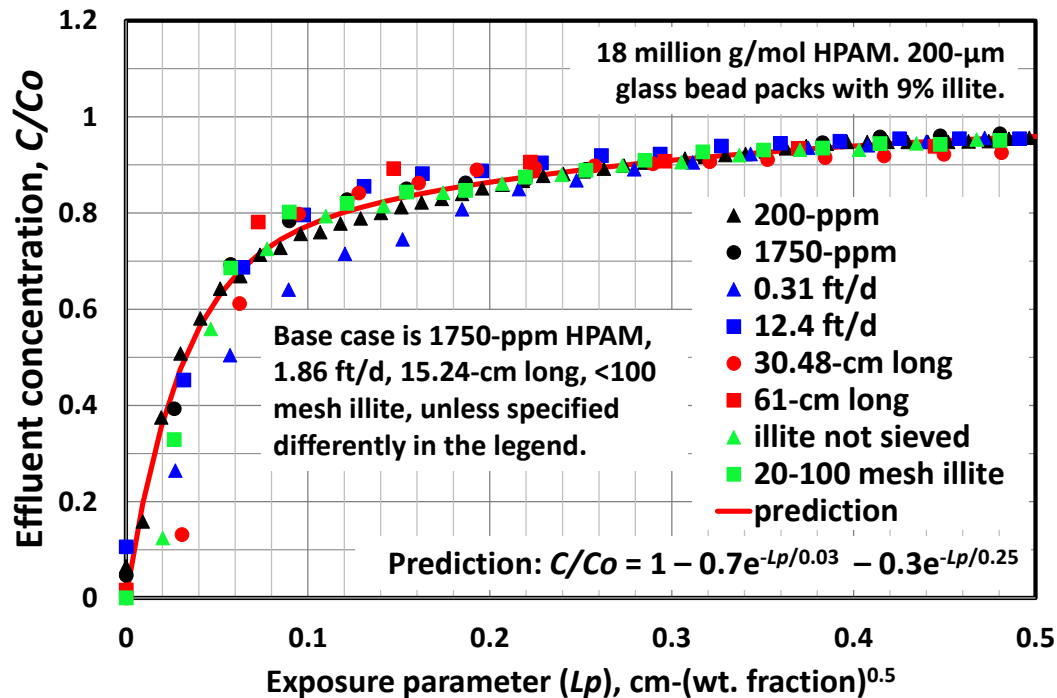


Figure 18—Match of experimental data with the double-exponential model.

Relevance to Field Results

Credible prediction of the performance of a polymer flood requires an accurate characterization of oil mobilization, which in turn requires an appropriate representation of polymer retention and propagation through the reservoir. As mentioned earlier, the standard Langmuir isotherm in simulators and the standard assumption of concentration-independent retention in fractional flow calculations cannot correctly describe polymer retention at the Milne Point polymer flood. Our findings suggest a similar concern for any polymer flood where significant levels of illite or kaolinite are present in the reservoir. Mineralogy analysis (especially for kaolinite and illite) is strongly encouraged to reveal whether the tailing phenomenon should be accounted for during simulations of polymer propagation/retention in a given field application.

At the Milne Point polymer flood, HPAM was first detected in both horizontal production wells (J-27 and J-28) after injecting only 10% PV (Dandekar et al. 2021). On the one hand, the fast polymer breakthrough is consistent with our experimental results in the sense that no delay in polymer propagation is evident due to retention. Also consistent with the experimental results, the maximum produced polymer concentration to date is 48% (in J-27) and 59% (in J-28) of the injected concentration. On the other hand, the fast polymer breakthrough is probably due to channeling through a fracture-like feature, rather than via propagation through typical Schrader Bluff reservoir sand. Given the near-unit-mobility displacement provided by the injected polymer solutions, breakthrough would not be expected before injection of 50% PV polymer solution. Thus, definitive field confirmation of the tailing effect will require significant additional time, PV injected, and analysis of produced polymer. As mentioned earlier, we anticipate that the tailing behavior should result in no significant delay in propagation of the polymer bank (and therefore the oil bank), but the effective viscosity and displacement efficiency may be less than originally planned. To reiterate a very positive note, produced water cuts dropped from ~70% during waterflooding before the project to less than 10% during polymer injection. To our knowledge, no other field polymer flood has resulted in this magnitude of reduction in water cut. At this time, only 15% PV of polymer has been injected, so there certainly is no delayed response to polymer injection.

Conclusions

1. Laboratory retention studies for the Milne Point polymer flood (North Slope of Alaska) consistently show virtually no delay in polymer propagation, a rapid rise in produced polymer to 70-90% of the injected concentration, followed by produced concentration gradually approaching the injected value over many pore volumes.
2. In contrast, conventional use of the Langmuir isotherm (used in most chemical flooding simulators) or concentration-independent polymer retention (used during fractional-flow calculations) predict a delay in propagation of the polymer front (in proportion to the given retention value), followed by a rapid rise in produced polymer concentration to the injected level.
3. From a practical viewpoint, this tailing behavior means that retention causes no significant delay in propagation of the polymer bank (and therefore the oil bank), but the effective viscosity and displacement efficiency is less than originally planned.
4. In Milne Point cores, the presence of the tailing phenomenon was not sensitive to flow rate, polymer concentration, core heterogeneity, or whether the core was preserved, cleaned of oil, or cleaned and re-saturated with oil, or cleaned, re-saturated and aged with oil.
5. The tailing phenomenon was also observed during mechanistic floods using glass bead packs when sufficient levels of kaolinite or illite were present. This observation was consistent with high levels of illite noted in Milne Point cores.
6. The tailing phenomenon was not noted during mechanistic floods that contained glass beads with montmorillonite, chlorite, calcium carbonate, dolomite, siderite, pyrite, or calcium sulfate.
7. The work suggests that mineralogy analysis (especially for kaolinite and illite) may reveal whether the tailing phenomenon should be accounted for during simulations of polymer propagation/retention in a given field application.
8. A model was proposed to account for the retention tailing phenomenon. Much of the retention data could be fitted to a double-exponential equation, where a relative short reaction (perhaps adsorption onto the outer surface of illite) accounted for ~70% of the HPAM retention and a longer reaction (perhaps associated with polymer penetration into the illite) accounted for the remaining ~30%.

Acknowledgements

We thank Baojun Bai, Abhijit Dandekar, Samson Ning, Brent Sheets, Yin Zhang, and the rest of the team associated with Department of Energy Award Number DE-FE0031606 for interesting discussions. Thanks also to Hilcorp for providing the oil and core material used in this work. We are also grateful to SNF for providing the polymers.

"This material is based upon work supported by the Department of Energy under Award Number DE-FE0031606."

Disclaimer: "This report was prepared as an account of work sponsored by an agency of the United States Government. Neither the United States Government nor any agency thereof, nor any of their employees, makes any warranty, express or implied, or assumes any legal liability or responsibility for the accuracy, completeness, or usefulness of any information, apparatus, product, or process disclosed, or represents that its use would not infringe privately owned rights. Reference herein to any specific commercial product, process, or service by trade name, trademark, manufacturer, or otherwise does not necessarily constitute or imply its endorsement, recommendation, or favoring by the United States Government or any agency thereof. The views and opinions of authors expressed herein do not necessarily state or reflect those of the United States Government or any agency thereof."

Nomenclature

- A_p = particle area, μm^2
 C = effluent concentration, mg/L or $\sim\text{ppm}$ [$\mu\text{g/g}$]
 C_o = injected concentration, mg/L or $\sim\text{ppm}$ [$\mu\text{g/g}$]
 C_p = effluent polymer concentration, mg/L or $\sim\text{ppm}$ [$\mu\text{g/g}$]
 C_{po} = injected polymer concentration, mg/L or $\sim\text{ppm}$ [$\mu\text{g/g}$]
 C_t = effluent tracer concentration, mg/L or $\sim\text{ppm}$ [$\mu\text{g/g}$]
 C_{to} = injected tracer concentration, mg/L or $\sim\text{ppm}$ [$\mu\text{g/g}$]
 C^* = polymer critical overlap concentration, mg/L or $\sim\text{ppm}$ [$\mu\text{g/g}$]
 d_s = surface diameter, $(A_p/\pi)^{1/2}$, μm
 d_v = volume diameter, $(6V_p/\pi)^{1/3}$, μm
 $D[3,2]$ = Sauter mean diameter, d_v^3/d_s^2 , μm
 $D[4,3]$ = d_v^4/d_s^3 , μm
 $Dv(10)$ = particle diameter below which accounts for 10% of the material volume, μm
 $Dv(50)$ = particle diameter below which accounts for 50% of the material volume, μm
 $Dv(90)$ = particle diameter below which accounts for 90% of the material volume, μm
 $IAPV$ = inaccessible pore volume
 k = permeability, darcys [μm^2]
 k_{wsor} = permeability to water at residual oil saturation, darcys [μm^2]
 Lp = exposure parameter in Eqs. 2 and 3, cm-(wt. fraction) $^{0.5}$
 M_{rock} = mass of rock in the sand pack, g
 M_w = polymer molecular weight, g/mol [daltons]
 PV = pore volumes of fluid injected
 ΔPV = pore volumes difference
 q_{qmb} = imbibition rate, cm^3/hr
 R_{pret} = polymer retention, $\mu\text{g/g}$
 S_{or} = residual oil saturation
 t = time, seconds
 tb = polymer breakthrough time in Eq. 2, seconds
 Δt = incremental time, hr
 u = darcy velocity, cm/s
 V_p = particle volume, μm^3
 ΔV = incremental effluent volume, cm^3
 ϕ = porosity
 ρ_{rock} = rock density, g/cm^3

References

- Chang, H., Zhang, Y., Dandekar, A.Y., Ning, S., Barnes, J.A., Edwards, R., Schulpen, W., Cerccone, D., Ciferno J. 2020. Experimental Investigation On Separation Behavior of Heavy Oil Emulsion for Polymer Flooding On Alaska North Slope. *SPE Production & Operations*, June 2020. doi.org/10.2118/200369-PA
- Dandekar, A., Bai, B., Barnes, J., Cerccone, D., Ciferno, J., Ning, S., Seright, R., Sheets, B., Wang, D., Zhang, Y. 2019. First Ever Polymer Flood Field Pilot - A Game Changer to Enhance the Recovery of Heavy Oils on Alaska's North Slope. Paper SPE 195257 presented at the SPE Western Regional Meeting, San Jose, California. 23-26 April. doi.org/10.2118/195257-MS.
- Dandekar, A., Bai, B., Barnes, J., Cerccone, D., Ciferno, J., Ning, S., ... Zhang, Y. 2020. First Ever Polymer Flood Field Pilot to Enhance the Recovery of Heavy Oils on Alaska's North Slope - Pushing Ahead One Year Later. Paper SPE 200814 presented at the SPE Western Regional Meeting, Bakersfield, California, USA, 27 April-1 May. doi.org/10.2118/200814-MS.
- Dandekar, A., Bai, B., Barnes, J., Cerccone, D., Ciferno, J., Edwards, R., Ning, S., Schulpen, W., Seright, R., Sheets, B., Wang, D., Zhang, Y. 2021. Heavy Oil Polymer EOR in the Challenging Alaskan Arctic - It Works! Paper URTEC presented at the Unconventional Resources Technology Conference held in Houston, Texas, USA, 26-28 July.
- Dawson, R., and Lantz, R.B. 1972. Inaccessible Pore Volume in Polymer Flooding. *SPE Journal* **12** (5): 448-452. SPE 3522-

- PA. doi.org/10.2118/3522-PA.
- Dhaliwal, A., Zhang, Y., Dandekar, A.Y., Ning, S., Barnes, J.A., Edwards, R., Schulpen, W., Cercone, D., and Ciferno, J. 2021. Experimental Investigation of Polymer Induced Fouling of Heater Tubes in The First Ever Polymer Flood Pilot On Alaska North Slope. *SPE Prod. & Oper* **36**(1): 70-82. doi.org/10.2118/200463-PA.
- Ferreira, V.H.S., and Moreno, R.B.Z.L. 2020. Polyacrylamide Adsorption and Readsorption in Sandstone Porous Media. *SPE Journal* **25**(1): 497-514. doi.org/10.2118/199352-PA.
- Gil, L., Gaillard, N., and Favero, C. 2015. Qualitative Determination of Polymer Presence by Flocculation. SNF Procedure QC-5065A. 16 October.
- Green, D.W., and Willhite, G.P. 2018. *Enhanced Oil Recovery*. Textbook Series, SPE, Richardson, Texas **6**: 2nd edition.
- Guetni, I., Marliere, C., Rousseau, D., Bihannic, I., Pelletier, M., and Villieras, F. 2019. Transport of HPAM Solutions in low Permeability Porous Media: Impacts of Salinity and Clay Content. Paper SPE 195434 presented at the SPE Europec featured at 81st EAGE Conference and Exhibition held in London, England, UK, 3-6 June. doi.org/10.2118/195434-MS.
- Home, R.N. Rodriguez, F. 1983. Dispersion in tracer flow in fractured geothermal systems. *Geophys. Res. Lett.* **1983**, 10, 289–292. doi.org/10.1029/GL010i004p00289.
- Jones, C.A., 2010. Engineering Properties of Resedimented Ugnu Clay from the Alaskan North Slope. Master of Science in Civil and Environmental Engineering thesis. Massachusetts Institute of Technology. June 2010, page 43.
- Jouenne, S. and Levache, B. 2020. Universal Viscosifying Behavior of Acrylamide-Based Polymers Used in Enhanced Oil Recovery. *Journal of Rheology* **64**(5) 1295-1313. doi.org/10.1122/8.0000063.
- Keller, W.D., Reynolds, R.C., Inoue, A. 1986. Morphology of Clay Minerals in the Smectite-to-Illite Conversion Series by Scanning Electron Microscope. *Clay and Clay Minerals* **34**(2): 187-197.
- Ma, S.M., Zhang, X., Morrow, N.R., and X. Zhou. 1999. Characterization of Wettability from Spontaneous Imbibition Measurements. *J Can Pet Technol* **38** (1999): doi.org/10.2118/99-13-49.
- Manichand, R.N., and Seright, R.S. 2014. Field vs Laboratory Polymer Retention Values for a Polymer Flood in the Tambaredjo Field. *SPE Res Eval & Eng.* **17**(3): 314-325. doi.org/10.2118/169027-PA.
- Mattax, C.C., and J.R. Kyte. 1962 Imbibition Oil Recovery from Fractured, Water-Drive Reservoir. *SPE J.* **2** (1962): 177–184. doi.org/10.2118/187-PA.
- Ning, S., Barnes, J., Edwards, R., Dunford, K., Eastham, K., Dandekar, A., ... Ciferno, J. 2019. First Ever Polymer Flood Field Pilot to Enhance the Recovery of Heavy Oils on Alaska's North Slope - Polymer Injection Performance. Paper URTEC:643 presented at the Unconventional Resources Technology Conference. Denver, Colorado, USA. 22-24 July. doi.org/10.15530/urtec-2019-643.
- Perkins, T.K., and Johnston, O.C. 1963 A Review of Diffusion and Dispersion in Porous Media. *SPE J.* **3** (1963): 70–84. doi.org/10.2118/480-PA.
- Rose, K., Boswell, R. Collett, T. 2011. Mount Elbert Gas Hydrate Stratigraphic Test Well, Alaska North Slope: Coring operations, core sedimentology, and lithostratigraphy. *Marine and Petroleum Geology* **28**(2011): 311-331. Doi.org/10.1016/j.marpetgeo.2010.02.001.
- Seright, R.S. 2017. How Much Polymer Should Be Injected during a Polymer Flood? Review of Previous and Current Practices. *SPE Journal* **22**(1): 1-18. doi.org/10.2118/179543-PA.
- Sugar, A., Serag, M., Torrealba, V.A., Buttner, U., Habuchi, S., Hoteit, H. 2021. Visualization of Polymer Retention Mechanisms in Porous Media Using Microfluidics. Paper SPE 200557 presented at the SPE Europec 82nd EAGE Conference and Exhibition. Amsterdam, The Netherlands. 14-17 June 2021. doi.org/0.2118/200557-MS.
- Wang, D., Zhang, J., Butler, R., and Olatunji, K. 2016. Scaling Laboratory-Data Surfactant-Imbibition Rates to the Field in Fractured-Shale Formations. *SPE Res Eval & Eng* **19** (3): 440–449. doi.org/10.2118/178489-PA.
- Wang, D., Li, C., and Seright, R.S. 2020. Laboratory Evaluation of Polymer Retention in a Heavy Oil Sand for a Polymer Flooding Application on Alaska's North Slope. *SPE Journal* **25**(4) 1842-1856. doi.org/10.2118/200428-PA.
- Wang, D., Namie, S., Seright, R.S. 2022. Pressure Barrier Applicability to Polymer Flood Design. Paper SPE 209462 presented at the SPE Virtual Improved Oil Recovery Conference. Tulsa, Oklahoma. 25-29 April. doi.org/10.2118/209462-MS.
- Wever, D.A Z., Bartlema, H., ten Berge, A.B.G.M., Al-Mjeni, R., and Glasbergen, G. 2018. The Effect of the Presence of Oil on Polymer Retention in Porous Media from Clastic Reservoirs in the Sultanate of Oman. Paper SPE 190430 presented at the SPE EOR Conference at Oil and Gas West Asia. Muscat, Oman. 26-28 March. doi.org/10.2118/190430-MS.
- Yang, Y., Liu, T., Li, Y., Li, Y., You, Z., Zuo, M., Diwu, P., Wang, R., Zhang, X., Liang, J. 2021. Effects of Velocity and Permeability on Tracer Dispersion in Porous Media. *Appli. Sci.* **2021**(11) 4411: 1-15. doi.org/10.3390/app11104411.
- Zhao, Y., Yin, S., Seright, R.S., Ning, S., Zhang, Y., and Bai, B. 2021. Enhancing Heavy-Oil-Recovery Efficiency by Combining Low-Salinity-Water and Polymer Flooding. *SPE Journal* **26**(3): 15350-01551. doi.org/10.2118/204220-PA.
- Zhang, G., and Seright, R.S. 2014. Effect of Concentration on HPAM Retention in Porous Media. *SPE Journal* **19**(3): 373-380. Paper 166256. doi.org/10.2118/166256-PA.

APPENDIX A—Particle Size Distributions

This Appendix shows particle size distributions for materials mentioned in the main body of the paper.

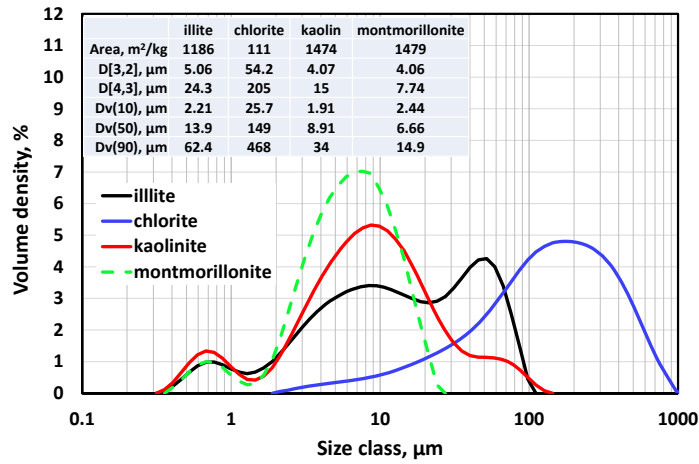


Figure A-1—Particle size distributions for four clays.

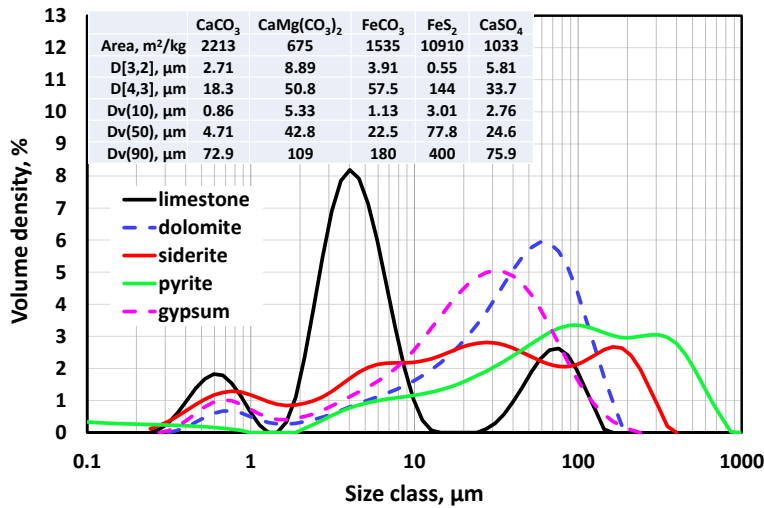


Figure A-2—Particle size distributions for five mineral additives.

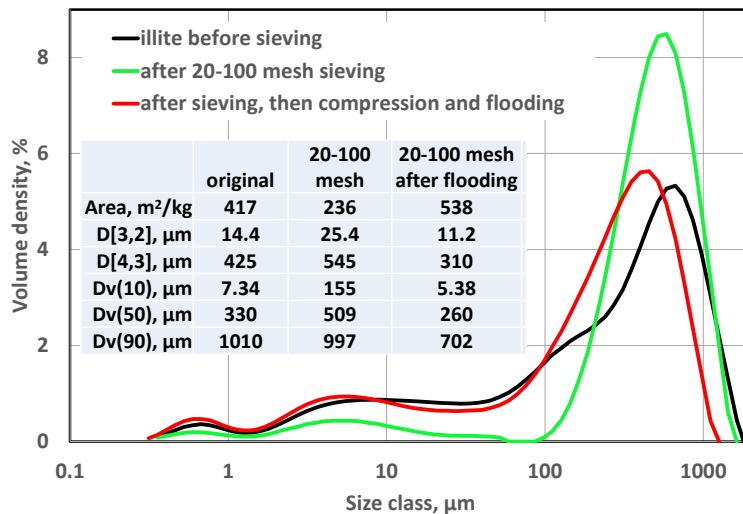


Figure A-3—Illite particle size distributions before and after compression and flooding.

APPENDIX B—Failed Mechanisms

This Appendix describes mechanisms that were examined, but could not adequately explain the experimental observations.

HPAM Imbibition into Illite.

We considered the possibility of polymer imbibition into the clay as an explanation for the tailing phenomenon. (Some previous papers on the imbibition process for oil, water, and/or surfactant include Mattax and Kyte 1962; Ma et al. 1990; and Wang et al. 2016.) In our cases with illite in the 200- μm bead packs (Figures 12, 13, 15 and 17), we estimated the rate of polymer solution imbibition into the illite by assuming that all HPAM retention (after polymer breakthrough) was attributed to polymer-solution imbibition into the clay. Consequently, for a given increment of effluent volume (ΔV), the rate of polymer-solution imbibition (q_{imb}) was given by Eq. B-1.

$$q_{imb} = \Delta V [(C_i/C_{i0}) - (C_p/C_{p0})] / \Delta t \dots\dots\dots (B-1)$$

where C_i/C_{i0} is the effluent tracer concentration relative to the injected tracer concentration, C_p/C_{p0} is the effluent polymer concentration relative to the injected polymer concentration, and Δt is the time increment during collection of that effluent sample. **Figure B-1** shows the results of these calculations associated with the data in Figures 12, 13, and 17. For a given curve, the rapid decline in imbibition rate with time could be rationalized as substantial increases in resistance to flow as the high-molecular-weight polymer attempts to penetrate further into the very small pores associated with the 0.4-md illite. However, many other observations are more difficult to explain using an imbibition model.

The three black curves in Figure B-1 reveal that the apparent rate of polymer imbibition into illite did not depend on the illite particle size. However, as discussed earlier, it is possible that the compression process (i.e., adding the 500-psi confining pressure) so that the particle size distributions were effectively the same for these three cases.

The black, green, and red curves with triangles in Figure B-1 show that the apparent imbibition rate was not sensitive to pack length (between 15.24 and 61 cm). This finding is counter-intuitive since the total illite surface area is proportional to pack length. So, one would expect the imbibition rate (in cm^3/hr at a given exposure time) to be four times as high for the 61-cm pack as for the 15.24-cm pack.

The light blue, black, and dark blue curves with circles in Figure B-1 show that the apparent imbibition rate increased substantially with increased flood rate between 0.31 and 12.4 ft/d. In fact, the curves in Figure B-1 could be almost be made to coincide if the time scale was divided by flood rate raised to the $2/3$ power. This finding is also counter-intuitive since one would expect the rate of polymer imbibition into the clay to be insensitive to the fluid velocity outside of the clay (assuming other conditions are fixed).

Figure B-2 shows the effect of illite concentration in the bead packs (between 4.5% and 36%). All cases here used 1.86 ft/d flood rate, were 15.24-cm long, and used 20-100-mesh illite. If the imbibition model was valid, we expected that the y-axis in Figure B-2 should be normalized by plotting the imbibition rate per gram of illite [(i.e., $\text{cm}^3/(\text{hr-g-illite})$]. However, Figure B-2 does not reveal an understandable relation between apparent imbibition rate with illite content in the pack.

In summary, the imbibition model does not provide a satisfactory explanation for the tailing phenomenon.

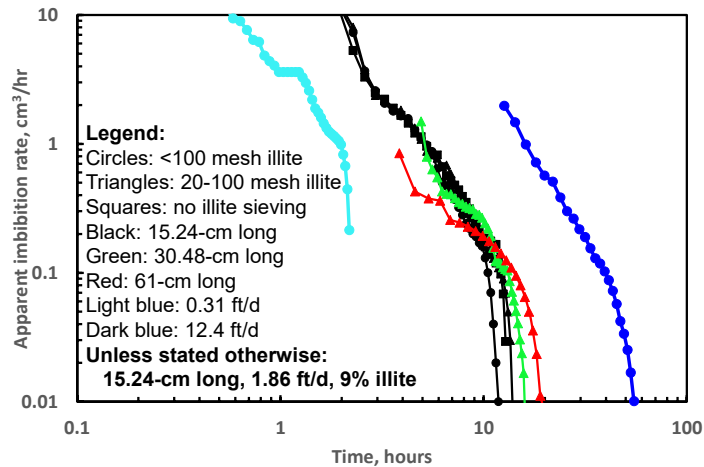


Figure B-1—Calculated imbibition into illite using Eq. 2 and Figures 12, 13, and 17.

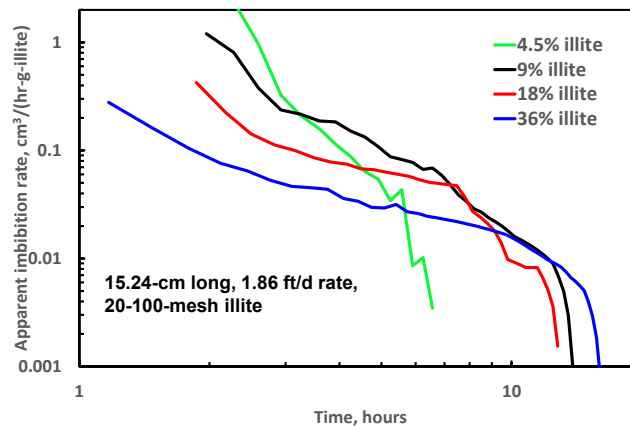


Figure B-2—Calculated imbibition into illite using Eq. 2 and Figure 15. (Effect of illite content).

Flocculation.

Clays are known to flocculate with certain clays. In fact, flocculation with kaolinite is a common (although not necessarily reliable) method to detect HPAM in polymer production wells (Gil et al. 2015; Wang et al. 2020). Since our illite was added as loose powder to the 200 μm beads, some illite particles may have become suspended in the flowing liquid during the flooding process—and subsequently flocculated with the HPAM. However, if this was a significant occurrence, one would expect pressures to increase substantially during flocculation (because of filtration of the flocculated clay within the bead pack). In contrast, for all floods described in this work, no external or internal plugging was observed during polymer flooding. For a fixed injection rate, injection pressures always increased rapidly (within about 1 PV) to the maximum value (at polymer breakthrough) that was not exceeded during the remainder of the multi-pore-volume injection process. Thus, clay flocculation with polymer does not appear to be responsible for the tailing phenomenon.

SI Metric Conversion Factors

cp x 1.0*	E-03	= Pa·s
ft x 3.048*	E-01	= m
in. x 2.54*	E+00	= cm
mD x 9.869 233 E-04		= μm^2
psi x 6.894 757 E+00		= kPa

* Conversion is exact.